Concrete Damage Plasticity Model for Modeling FRP-to-Concrete Bond Behavior

Y. Tao [1] and J.F. Chen [2]

ABSTRACT: The technique of externally bonding fiber reinforced polymer (FRP) composites has become very popular worldwide for retrofitting existing reinforced concrete (RC) structures. Debonding of FRP from the concrete substrate is a typical failure mode in such strengthened structures. The bond behavior between FRP and concrete thus plays a crucial role in these structures. The FRP-to-concrete bond behavior has been extensively investigated experimentally, commonly using the single or double shear test of FRP-to-concrete bonded joint. Comparatively, much less research has been concerned with the numerical simulation, chiefly due to difficulties in the accurate modeling of the complex behavior of concrete. This paper presents a simple but robust finite element (FE) model for simulating the bond behavior in the entire debonding process for the single shear test. A concrete damage plasticity model is proposed to capture the concrete-to-FRP bond behavior. Numerical results are in close agreement with test data, validating the model. In addition to accuracy, the model has two further advantages: it only requires the basic material parameters (i.e. no arbitrary user defined parameter such as the shear retention factor is required) and it can be directly implemented in the FE software ABAQUS.

KEYWORDS: Fiber reinforced polymer; Concrete; Bond; Finite element model; Damage.

---

[1] Associate Professor, School of Civil Engineering, Xi'an University of Architecture and Technology, China.
[2] Professor of Civil and Structural Engineering, School of Planning, Architecture, and Civil Engineering, Queen's University Belfast, UK. Email: j.chen@qub.ac.uk.

INTRODUCTION

Externally bonding fiber reinforced polymer (FRP) has been widely used to strengthening and retrofit existing concrete structures (Teng et al., 2002). One of the main failure modes of flexurally and shear strengthened concrete structures is the debonding failure of the externally bonded FRP (Chen and Teng, 2001; Teng et al., 2002). This has led to extensive research on the bond behavior between FRP and concrete in the last two decades. This bond behavior is typically investigated experimentally using the 'shear' test of FRP-to-concrete bonded joints where a FRP plate is bonded to a concrete block and subjected to a tensile force (e.g. Ali-Ahmad et al., 2006; Benzarti et al. 2011; Täljsten, 1996; Wu et al., 2001; Yao et al., 2005). Typical debonding failure in the shear test occurs in the concrete a small distance, usually 2-5 mm, away from the adhesive-concrete interface. The bond behavior is thus usually controlled by the behavior of the concrete. In addition to experimental studies, the bond characteristics of the FRP-to-concrete interface have also been investigated in a number of analytical (e.g. Chen et al., 2007; Yuan et al., 2004); and numerical (e.g. Chen and Pan, 2006; Coronado and Lopez, 2007; Diab and Wu, 2007; Lu et al., 2005b; Lu et al., 2006; Pham and Al-Mahaidi, 2007; Benvenuti et al. 2012; Marfia et al. 2012;) studies. A brief review of existing finite element (FE) modeling of the FRP-to-concrete bond behavior is presented as follows.

Existing FE studies on the FRP-to-concrete bonded joint are summarized in Table 1. They may be classified into three approaches: a) direct modeling approach where the behavior of concrete is accurately modeled in meso-scale with an appropriate constitutive model (e.g. Lu et al., 2005b; 2006); b) interface modeling approach where the bond behavior is modeled using a layer of interface elements (e.g. Diab and Wu, 2007); and c) crack band modeling approach where the debonding failure is assumed to take place within a band in the concrete

adjacent to the FRP-concrete interface with a modified constitutive law for this band (e.g. Coronado and Lopez, 2007; 2010). Note that this 'crack band' approach is fundamentally different from Bažant and Oh's (1983) 'crack band theory' which is discussed in more detail in the next section.

In the direct modeling approach, a meso-scale FE mesh, with the smallest element size commonly in the range of 0.5~2 mm, is adopted to model the detailed behavior of concrete near the FRP-to-concrete bondline so that the bond-slip behavior can be obtained. Lu et al. (2005b) adopted a fixed angle crack model and a shear retention model for the concrete. The bond-slip model (Lu et al., 2005a) developed based on Lu et al. (2005b) has been very widely accepted by the research community (e.g. Godat et al. 2007; Smith and Gravina 2007; Obaidat et al. 2010; Chen et al., 2012;). Lu et al. (2006) later adopted a rotation angle crack model in conjunction with a user-defined constitutive model for concrete. Both FE models were implemented through a user-subroutine in MSC.MARC (2003). The predictions are also sensitive to the choice of the shear retention model. Pham and Al-Mahaidi (2007) directly adopted the concrete model in DIANA (2003). Their concrete mesh consisted of a transition layer with element size varying from 2 to 10 mm and a coarse layer with 10 mm elements. It appears that the effect of the thickness of the fine layer was unclear but it could be significant as the predicted concrete cracks propagated into both layers. All these studies adopted the smeared crack model of concrete. A number of studies (e.g. Camata et al., 2004; Pham et al., 2006) have attempted to combine both the smeared and discrete crack models. However, this approach usually requires to predefine the crack locations and an additional interface crack model to define the discrete crack behavior, making it difficult to be predictive.

The interface model approach is most commonly adopted for modeling FRP strengthened structures (e.g. Chen et al., 2011; Chen et al., 2012) or for modeling three-dimensional

behavior (Salomoni et al., 2011) because it is unrealistic to model the whole strengthened structure in 3D using meso-scale elements due to heavy computational demands. The FRP-to-concrete interface is usually represented by zero thickness interface elements (e.g. Diab and Wu, 2007; Salomoni et al., 2011). A constitutive law for the interface elements is needed to obtain from either the direct model approach or shear tests. This is thus not really a predictive approach for the bond behavior (but for structural behavior).

The crack band approach assumes that debonding occurs within a thin band in the concrete adjacent to the adhesive-to-concrete interface, and the properties of the concrete within this band are different from the nearby plain concrete because of the ingression of adhesive (Coronado and Lopez, 2007; 2008). Consequently, a modified concrete constitutive law is required for this band (Coronado and Lopez, 2007; 2010), but its properties include fracture energy, size effect fracture energy and tensile strength, need to be determined experimentally. It is thus debatable whether the approach is predictive. Furthermore, the properties can be significantly affected by the adopted adhesive, rendering the approach more complex for practical applications. Also, if the band represents the thin layer of concrete with adhesive ingression, it is debatable whether failure would still occur within this stronger layer because the adhesion leads to a higher tensile strength of concrete.

Based on the above discussion, it may be concluded that the direct modeling approach is the most appropriate for modeling the FRP-to-concrete bond behavior as a truly predictive model. However, numerical studies on the bond behavior using this approach have been very limited mainly because of challenges in the accurate modeling of concrete.

This paper presents a predictive FE model using the direct modeling approach. A new damage model based on the plastic degradation theory is first proposed. It is then incorporated in the

concrete damage plasticity model in ABAQUS for FE simulation of the FRP-to-concrete bonded joint test. Predictions of the proposed FE model are compared with test results and predictions of existing concrete damage models.

MODELING OF CONCRETE

Modeling of concrete fracture

Two methods are commonly used in FE modeling of concrete cracking: the discrete crack model and the smeared crack model (Rots, 1991). In the former, a crack is treated as a geometrical identity so it is either pre-embedded in the FE mesh (Yang et al. 2009) or through continuous re-meshing (Yang et al., 2003; Yang and Chen 2005). The latter keeps the geometry (and thus the mesh) unchanged and the cracking is modeled through the concrete constitutive law (Rots, 1991). The smeared crack approach is adopted in this study as it is impossible to track numerous micro-cracks in the single shear test where failure occurs within a few millimeters (usually 2~5 mm) in the concrete adjacent to the bondline.

One of the drawbacks of the smeared concrete model is that it involves the strain localization phenomenon due to strain-softening, where the energy consumption approaches to zero during crack propagation when the element size approaches to zero (Bažant and Jaime, 1998), leading to results sensitive to the FE mesh. Bažant and Oh's (1983) crack band theory is adopted in this study to overcome the mesh sensitivity problem. The theory relates the crack opening width w, the width of the crack band h and the crack strain ε_{ct} through:

$$w = h\int \varepsilon_{ct} \tag{1}$$

The crack band width *h* represents the effective width of the fracture process zone over which micro-cracks are assumed to be uniformly distributed. In the FE analysis, the cracking strain is assumed to be uniformly distributed over *h* in an element which is referred as the characteristic length of an element and is related to the element size, type and integration scheme (Rots 1991).

Compressive and tensile behavior of concrete

In this paper, the concrete is modeled using the concrete damage plasticity model available in ABAQUS (2007). The plasticity model adopts the yield function proposed by Lubliner et al. (1989) and modified by Lee and Fenves (1998), and follows a non-associated flow rule. The concrete under uniaxial compression is described by the following stress strain relationship proposed by Saenz (1964):

$$\sigma_c = \frac{E_0 \varepsilon_c}{1 + \left(\frac{E_0 \varepsilon_p}{\sigma_p} - 2 \right) \left(\frac{\varepsilon_c}{\varepsilon_p} \right) + \left(\frac{\varepsilon_c}{\varepsilon_p} \right)^2} \tag{2}$$

where σ_c and ε_c are respectively the compressive stress and strain, σ_p and ε_p are the experimentally determined maximum stress and its corresponding strain which are taken to be the cylinder strength f_c' (MPa) and 0.002 respectively in this study. The elastic modulus of the concrete E_0 is estimated from $E_0 = 4730\sqrt{f_c'}$ (MPa) following ACI 318 (2002).

Under uniaxial tension, the problem involves tensile cracking. The fracture energy G_F, that is the energy required to create a unit area of stress free crack surface which is size independent, instead of the descending branch of the stress-strain curve which is size dependent, is treated as a material property of the concrete. In this paper, the stress-crack opening displacement relationship proposed by Hordijk (1991) is adopted:

$$\frac{\sigma_t}{f_t} = \left[1 + \left(c_1 \frac{w_t}{w_{cr}}\right)^3\right] e^{\left(-c_2 \frac{w_t}{w_{cr}}\right)} - \frac{w_t}{w_{cr}}\left(1 + c_1^3\right) e^{(-c_2)} \tag{3}$$

$$w_{cr} = 5.14 \frac{G_F}{f_t} \tag{4}$$

where w_t is the crack opening displacement, w_{cr} is the crack opening displacement at the complete loss of tensile stress, σ_t is the tensile stress normal to the crack direction, f_t is the concrete uniaxial tensile strength, and c_1=3.0 and c_2 =6.93 are constants determined from tensile tests of concrete. The CEB-FIB (1991) model is used in this paper to estimate f_t and G_F:

$$f_t = 1.4\left(\frac{f_c' - 8}{10}\right)^{\frac{2}{3}}, \text{MPa} \tag{5}$$

$$G_F = \left(0.0469 d_a^2 - 0.5 d_a + 26\right)\left(\frac{f_c'}{10}\right)^{0.7}, \text{N/mm} \tag{6}$$

where d_a is the maximum aggregate size of the concrete. In the present study, d_a is assumed to be *20 mm* if no test data is available. Once the stress-crack opening displacement relationship is known, the stress-strain relationship can be determined for each element based on its size through Eq. 1. The Poisson's ratio v=0.2 is assumed in this study.

CONCRETE DAMAGE MODELS

General

The nonlinear behavior of concrete is attributed to the process of damage and plasticity. The process of damage can be attributed to micro-cracking, coalescence and decohesion etc. The

plasticity behavior can be characterized by several phenomena such as strain softening, progressive deterioration and volumetric expansion etc. These lead to the reduction of the strength and stiffness of concrete (Cicekli et al., 2007; Grassl and Jirásek, 2006; Lubliner et al., 1989). Damage is usually characterized by the degradation of stiffness. An isotropic scaled damage model from the continuum damage mechanics is introduced in ABAQUS (2007) to describe the stiffness degradation, which can be represented by Eq. 7 under uniaxial loading:

$$\sigma = (1-d)E_0\left(\varepsilon - \varepsilon^{pl}\right) \tag{7}$$

where σ, ε, and ε^{pl} represent respectively the stress, total strain and plastic strain; E_0 is the initial (undamaged) elastic stiffness and d the damage factor, which characterizes the degradation of the elastic stiffness and has values in the range between 0 (undamaged) to 1 (fully damaged). The current degraded stiffness E is defined as:

$$E = (1-d)E_0 \tag{8}$$

If no damage is considered in the concrete (d=0), Eq. 7 is reduced to:

$$\sigma = E_0\left(\varepsilon - \varepsilon^{pl}\right) \tag{9}$$

in which the plastic stain (ε^{pl}) is the same as that without stiffness degradation (ε^{p}) (Fig. 1b).

Stiffness degradation models can be classified into two types according to the presence of irreversible deformation/plastic strain: elastic degradation models and plastic degradation models (Lubliner et al. 1989). The elastic degradation models are associated with the total strain, implying that no plastic strain exists ($\bar{\varepsilon}^{p} = \varepsilon^{p} = 0$, where $\bar{\varepsilon}^{p}$ is the plastic strain with

stiffness degradation), so the unloading branch passes through the origin (Fig. 1). Eq. 7 in this case can be rewritten as:

$$\sigma = (1-d)E_0\varepsilon \tag{10}$$

where ε is the total strain. Lubiner et al. (1989) stressed that the concept of elastic degradation is associated with the total deformation but without the necessity of a damage criterion. A plastic degradation, in which the stiffness degradation is associated with the plastic deformation instead of the total deformation, was introduced to overcome the weaknesses of the elastic degradation model (Lubiner et al. 1989). It means that irreversible deformation/plastic strain exists after damage has occurred (so the plastic strain with stiffness degradation $\bar{\varepsilon}^p \neq 0$) (Fig. 1b). Eq. 7 in this case can be rewritten as:

$$\sigma = (1-d)E_0\left(\varepsilon - \bar{\varepsilon}^p\right) \tag{11}$$

Lubliner et al.'s (1989) damage model

Lubliner et al. (1989) proposed a simple damage model that plastic degradation occurs only in the softening range and the stiffness is proportional to the cohesion of the material:

$$\frac{E}{E_0} = \frac{c}{c_{\max}} = 1-d \tag{12}$$

$$d = 1 - \frac{c}{c_{\max}} \tag{13}$$

where c is the cohesion in the yield criteria which is proportional to stress and c_{max} is proportional to the strength of the concrete (Lubliner et al. 1989). Under uniaxial tension or compression, Eq. 13 reduces to:

$$d = 1 - \frac{\sigma}{f} \tag{14}$$

in which f is either the tensile or compressive strength of concrete as appropriate. Based on the geometry in Fig. 1b, $\bar{\varepsilon}^p$ can be related to the damage factor d as:

$$\bar{\varepsilon}^p = \varepsilon^p - \frac{d}{(1-d)}\frac{\sigma}{E_0} \tag{15}$$

Substituting Eq. 14 into Eq. 15 yields

$$\bar{\varepsilon}^p = \varepsilon - \frac{\sigma}{E_0} - \frac{f-\sigma}{E_0} = \varepsilon - \frac{f}{E_0} \tag{16}$$

in which f/E_0 is the elastic strain at the peak stress. Therefore, it is observed in this study that in Lubliner et al.'s (1989) damage model the elastic strain remains constant (f/E_0) after the peak stress.

Damage models used for simulating FRP strengthened concrete structures

Several concrete damage models have been used to simulate FRP strengthened concrete structures. Chen et al. (2011) adopted the classical elastic damage model to describe the tensile behavior of concrete in the modeling of FRP strengthened reinforced concrete (RC) beams, assuming that there is no plastic strain ($\bar{\varepsilon}^p = 0$) throughout the post-cracking range so the unloading paths of the stress-strain curve always pass through the origin of the coordinate system in Figs 1 and 2. Yu et al. (2010) assumed that the elastic strain is constant after the peak stress in compression in the modeling of FRP confined concrete columns, which is proved above the same as the damage model proposed by Lubliner et al. (1989). Chen et al.

(2012) used Rots' (1988) shear retention model for the modeling of FRP shear-strengthened RC beams:

$$\beta = \left(1 - \frac{\varepsilon_{cr}}{\varepsilon_{cr,u}}\right)^n \tag{17}$$

where ε_{cr} is the concrete crack strain corresponding to w_t in Eq. 3, $\varepsilon_{cr,u}$ is the concrete cracking strain at the complete loss of stress corresponding to w_{cr} in Eq. 3, and the power n controls the rate of shear degradation.

A new damage model

Lubliner et al.'s (1989) and the other damage models summarized above were implemented to simulate the bond behavior in the single shear test but they did not lead to reasonable predictions in comparison with test data. A new model was thus proposed in this study.

Once the concrete enters into the softening range, the stiffness is degraded resulting in a plastic strain degradation (so $\bar{\varepsilon}^p \le \varepsilon^p$, see Fig. 1a). Instead of assuming that the stiffness is proportional to the cohesion of the material as in Lubliner et al. (1989), it is assumed here that the ratio of the plastic strain with stiffness degradation ($\bar{\varepsilon}^p$) to that without stiffness degradation (ε^p), k, is proportional to the ratio of cohesion to the maximum cohesion of the material. The rational of this assumption is that the plastic strain with stiffness degradation must be smaller than that without degradation, and the effect increases as degradation increases. However, the total plastic strain shall not reduce as deformation increases.

In the case of uniaxial loading, this ratio can be expressed as:

$$k = \frac{\bar{\varepsilon}^P}{\varepsilon^P} = \frac{c}{c_{\max}} = \frac{\sigma}{f} \qquad \text{subject to} \quad \dot{\bar{\varepsilon}}^P \geq 0 \tag{18}$$

Note that Eq. 18 is subject to the condition that the plastic strain rate is not negative ($\dot{\bar{\varepsilon}}^P \geq 0$) because within the entire cracking process, the plastic strain cannot decrease as crack widens. Although this condition would theoretically break down at a certain point because Eq. 18 implies that $\bar{\varepsilon}^P = 0$ when σ = 0, it is actually satisfied in the entire range for all cases covered in this study in tension. This is because ABAQUS does not allow the stress σ to reduce below 1% of the strength *f* in both tension and compression for numerical stability. In compression, this condition is more likely violated at large strains, especially for high strength concrete.

Assuming that the condition is not satisfied (i.e. when the adoption of *k* leads to an decrease of the plastic strain so $\bar{\varepsilon}^P{}_{(i+1)} < \bar{\varepsilon}^P{}_{(i)}$) after deformation has developed to certain value, and the elastic strain at the moment when the condition starts to be violated (at $\dot{\bar{\varepsilon}}^P = 0$) is $\bar{\varepsilon}^e_{cr}$, the damage factor is calculated thereafter by assuming that the elastic strain remains constant at $\bar{\varepsilon}^e_{cr}$. This is somewhat similar to Lubliner et al.'s (1989) model but note that the constant elastic strain is different here. From Fig. 1b:

$$\bar{\varepsilon}^P = \varepsilon - \bar{\varepsilon}^e_{cr} = \varepsilon^P - \frac{d}{1-d} \cdot \frac{\sigma}{E_0} \tag{19}$$

So the damage factor

$$d = \frac{\varepsilon^P - (\varepsilon - \bar{\varepsilon}^e_{cr})}{\varepsilon^P - (\varepsilon - \bar{\varepsilon}^e_{cr}) + \dfrac{\sigma}{E_0}} \tag{20}$$

Implementation of the proposed damage model in ABAQUS

In ABAQUS, the relationship between the plastic strain without stiffness degradation, ε^p, and the damage factor d needs to be defined by the user as a constitutive law of concrete. Therefore, the relationship between k in Eq. 18 and the damage factor d needs to be established in order to implement the new damage model in ABAQUS. The plastic strain with stiffness degradation $\bar{\varepsilon}^p$ can be related to the damage factor d using Eq. 15. Substituting Eq. 18 into Eq. 15 and combining Eq. 20 gives

$$d = \begin{cases} \dfrac{(1-k)\varepsilon^P}{(1-k)\varepsilon^P + \sigma/E_0} & \text{if } \dot{\bar{\varepsilon}}^P \geq 0 \\ \dfrac{\varepsilon^P - (\varepsilon - \bar{\varepsilon}^e_{cr})}{\varepsilon^P - (\varepsilon - \bar{\varepsilon}^e_{cr}) + \sigma / E_0} & \text{if } \dot{\bar{\varepsilon}}^P < 0 \end{cases} \tag{21}$$

Figure 2 shows a typical stress-strain curve for concrete under uniaxial tension, where the subscript t represents tension. The stress-crack strain curve for a given element can be obtained from the stress-crack opening displacement curve (Eq. 3) depending on the element type and size through Eq. 1. The relationship between the crack strain $\varepsilon_t^p = w_t/h$ and tension damage factor d_t can then be calculated from Eq. 21.

The compression damage is assumed to follow the same rule as in tension in this study. The compression damage factor d_c versus compressive plastic strain ε_c^p can be calculated from Eq. 21. Note that the compressive plastic strain is calculated from $\varepsilon_c^p = \varepsilon_c - \sigma_c/E_0$. Damage is assumed to occur only after the concrete enters softening in both tension and compression.

FE MODELING OF SINGLE SHEAR TEST OF FRP-TO-CONCRETE BONDED JOINTS

Geometry

A 45 mm thick concrete prism as shown in Fig. 3 has been modeled as a plane stress problem in the FE analysis. This thickness is smaller than most specimens in experiments but the rest of the concrete should have little effect on the FE results as the test commonly fails by debonding in concrete a few millimeters away from the FRP-to-concrete interface and only this failure mode is concerned in this study. The geometry of the FE model is the same as that adopted by Lu et al. (2005b; 2006). In the FE model, the specimen was restrained vertically along the base and horizontally along part of the right edge h_s (Fig. 3). For specimens with a free height h_c smaller than 30 mm, the actual h_c value was used. For specimens with h_c greater than 30 mm, h_c was set to 30 mm. The thickness of the FRP plate t_p was set equal to 1 mm but the modulus of elasticity of the plate E_p was modified so that the FRP plate had the actual axial stiffness $E_p t_p$.

Constitutive models and FE mesh

As aforementioned, the concrete damage plasticity model was used to describe the concrete behavior in this study. The plastic behavior of concrete was modeled following the compressive and tensile behavior described earlier. The damage was modeled using the damage model proposed in this study. The FRP was modeled as a linear elastic material.

The concrete was modeled using square elements with four integration points (CPS4) in this study. All concrete elements had the same size. Rots' (1988) recommendation was adopted

that the characteristic length for a square element with 4 integration points is $\sqrt{2}e$ where e is the element side length. The FRP was modeled using the same element with matching mesh.

Interpretation of numerical results

Because the test was modeled as a plane stress problem while the actual behavior is three dimensional (Chen and Pan 2005), the predicted load, displacement, stress and strain in the FRP plate were all adjusted following the width ratio factor β_w proposed by Chen and Teng (2001):

$$\beta_w = \sqrt{\frac{2 - b_f / b_c}{1 + b_f / b_c}} \tag{22}$$

where b_f and b_c are the widths of the FRP plate and the concrete prism respectively.

Mesh convergence analysis

Specimen II-5 reported in Yao et al. (2005) was used as a reference case for conducting the mesh convergence study. Four meshes with concrete element size equal to 5, 2, 1 and 0.5mm were considered. Figures 4a and b show respectively the predicted load-slip curves and the loading capacity from these meshes. The predicted ultimate load increases slightly as the mesh size reduces. This is different from the normal smeared crack model where the loading capacity is expected to reduce as mesh size reduces because the energy consumed by the cracking elements reduces with element size, leading to mesh dependent results. The difference in the loading capacity between the 0.5 mm mesh and the 1 mm mesh is 2.8% (Fig. 4b), showing that the mesh sensitivity problem is effectively eliminated by adopting the crack band theory and mesh convergence is achieved. These four meshes and the predicted damage contours at debonding are shown in Fig. 5. The 5 mm mesh is too coarse: it predicts a uniform

5 mm (one element) concrete damage (debonding) underneath the FRP along the length of the FRP and a wedge failure of the concrete at the right. The other three meshes predicted the same failure mode and almost the same concrete damage area, with small inclined concrete cantilevers as in Lu et al. (2005b). On balance of accuracy and computational economy, the 1 mm mesh was adopted for all cases reported in the rest of the paper.

INFLUENCE OF CONCRETE DAMAGE MODEL

The proposed together with the other concrete damage models described early were used to investigate their effects on the FE predictions. A model without considering any damage, i.e. both $d_t = d_c = 0$, was also considered as a reference. Figures 6 and 7 show how the damage factor varies respectively with the crack strain (in tension) or inelastic strain (in compression) for these models, where a 1 mm square element and concrete properties for specimen II-5 in Yao et al. (2005) were used.

Figures 8a and b show respectively the predicted load-slip curves for specimen II-5 in Yao et al. (2005) and No. 1 in Ali-Ahmad et al. (2006) using the different damage models. It is seen that different concrete damage models produce significantly different results. The predictions from the present model are clearly in closer agreement with the test results than other models. It may be noted that the damage model has almost no effect in the early stage (<2 kN in Fig. 8a and <4 kN in Fig. 8b). This is because at this stage the concrete is almost all elastic so little damage has occurred anyway. The simulation using Chen et al.'s (2011) model was terminated earlier for both specimens due to convergence difficulties. The results appear to show that Lubliner et al.'s (1989) damage model as adopted by Yu et al. (2010) over-estimates the bond strength if only tensile damage is considered, but under-estimates if the damage model is applied in both tension and compression. The model without considering

any damage in both tension and compression under-estimates the loading capacity. These results show that the inclusion of compression damage has a significant effect on the prediction, which may be explained by Lu et al.'s (2005b) findings. The shear forces on the inclined meso-cantilevers, which are caused by the formation of interfacial shallow cracks near the bond interface, resulting in a combined compression and bending at the root of the cantilevers leading to either crushing failure, or flexural failure at the root.

The damage model based on Rots (1988) shear retention model with n=5 also over-estimates the loading capacity (Fig. 8). The effect of the value of n on the prediction is shown respectively in Figs 9a and b for the two specimens: a smaller n value leads to smaller predictions in both load and slip and the effect is very significant. It is seen that the prediction with n=0.5 is close to the test results for specimen II-5 in Yao et al. (2005) but that with n=1 is closer for specimen No. 1 in Ali-Ahmad et al. (2006). It is thus not possible to choose a specific value for prediction purpose.

COMPARISON OF FE PREDICTIONS WITH TEST RESUTLTS

The proposed FE model has been used to simulate all the 56 single shear tests reported in Yao et al. (2005) in which all the geometrical and material properties necessary for FE modeling are available. It may be noted that Yao et al. (2005) reported a total of 72 tests but 16 of them failed in other modes rather than debonding in concrete so they were excluded in this study. The concrete cylinder strength for the specimens in Yao et al. (2005) varied from 19 to 27 MPa. To increase the range of concrete strength, specimen No. 1 from Ali-Ahmad et al. (2006) and three specimens (S-CFS-400-25) from Wu et al. (2001) were further simulated. The concrete cylinder strength was respectively 38 MPa for the former and 57.6 MPa for the

latter. Figure 10 shows that the FE predictions are overall in very close agreement with the 60 test data.

Three typical specimens with different concrete strength are chosen from the above database for further comparison between the FE prediction, test data and analytical solution if available. These are specimen II-5 in Yao et al. (2005), specimen No. 1 in Ali-Ahmad et al. (2006) and specimen S-CFS-400-25 in Wu et al. (2001), which had concrete strength of 23, 38 and 57.6 MPa respectively. Figures 11 and 12 show that the predicted and measured load-slip curves are in close agreement for the first two specimens (that for the third one is not available). Yuan et al. (2004) analyzed the load-slip curve for specimen II-5 in Yao et al. (2005) using their analytical solution. Their results are also shown in Fig. 11 for comparison. Figure 13 shows the close agreement between the predicted and measured FRP strain distribution for the third specimen. Table 2 compares the loading capacities from FE prediction, test and Chen and Teng's (2001) bond strength model. It shows that the loading capacities from the present FE prediction are in close agreement with test and those predicted from Chen and Teng's (2001) model.

Figure 14 shows a comparison between the FE prediction, test and Yuan et al.'s (2004) analytical solution of FRP axial stress at Point B, E and G as marked in Fig. 11. The axial stress is used here because it was used in Yuan et al. (2004). The test axial stress was obtained by multiplying the measured strain on the top surface by the Young's modulus of the FRP. There is a very close agreement between the three when the bonded joint is almost entirely elastic at Point B with load P = 2.26 kN. At the initiation of debonding (at Point E with P = 5.53 kN), the FE prediction is in good agreement with the analytical solution. The test results are in agreement with the other two in overall trend, but shows large fluctuations. This is probably caused by local bending of the FRP (see Chen et al. 2001), in addition to probable

measurement errors. Point G (P = 5.74 kN) corresponds to a state when debonding has propagated by 55 mm from the loaded end. The analytical strain is constant within this 55 mm. The strain from FE prediction is the largest at the loaded end and reduces gradually within the debonded zone, although it is overall in agreement with the analytical solution. The cause for this phenomenon will be discussed below. Again, the test strain shows large fluctuations but is in agreement with the other two in trend.

Figure 15 shows the predicted load-slip curves for group VII specimens in Yao et al. (2005) whose bond length varied but all other parameters remained the same. The effective bond length, which is defined as the bond length beyond which the ultimate load does not increase with an increase of the bond length, calculated by Chen and Teng's (2001) model is 92 mm for this group, implying that the ultimate load of this group should be constant because the bond lengths were greater than the effective bond length for all specimens in the group. Although the FE predicted ultimate load capacities are more or less the same (Fig. 15), they do show a trend that the loading capacity increases slowly with the bond length. This phenomenon is evident from test results as shown in the inert table in Fig. 15.

The above phenomenon is consistent with the phenomenon in Fig. 11 that the load continues to increase slowly after the initiation of debonding (Point E), instead of a horizontal plateau as predicted by Yuan et al.'s (2004) analytical solution. This is also consistent with the phenomenon in Fig. 14 that the FE predicted FRP stress is not constant within the debonded zone: it is the highest at the loaded end and reduces slowly within the zone towards the debonding front. This phenomenon may be explained by the different material constitutive models employed in the different analyses. Typically a bi-linear bond-slip model is assumed in analytical analyses such as Yuan et al. (2004). The bi-linear bond-slip model assumes that the interface does not resist any stress once the slip exceeds the critical value, leading to a

horizontal plateau when the bond length is sufficiently large. In the present FE analysis, although the tensile and compressive stresses are also supposed to reduce to zero when the strain reaches a critical value (Figs 1 and 2), ABAQUS (and many other FE packages) does not allow the tensile stress to fall below 1% of f_t to ensure numerical stability (similar in compression). This means that concrete always has a small residual strength in both tension and compression in the FE mode. Therefore, the difference between the analytical solution and the FE prediction is most likely due to the differences in the assumptions adopted. Although it may be argued that the slow increase of the FE predicted loading capacity with an increase of the bond length is also due to the arbitrary numerical treatment, it is evident in the test data as in Figs 11, 14 and 15 that the load increases slowly with deformation even at large slips.

For specimen II-5 in Yao et al. (2005), a number of points on the FE load-slip curve (marked Point A-I in Fig. 11) were chosen to investigate the debonding process. Figure 16 shows the tensile damage contours in the concrete. It may be noted that the tensile damage is directly related to the cracking strain so these contours represent closely the crack pattern in the concrete, so the progressive development of damage in Fig. 16 also represents closely the propagation of concrete crack/FRP debonding.

The concrete near the loaded end exhibits softening in a small zone directly under the FRP when the load is about 30% of the ultimate load (Fig. 16b). The length of this small softening zone has been about doubled and its depth significantly increased when the load increases to about 60% (Fig. 16d). Micro-cracks start to form with an angel of about 45° to the horizontal. A macro crack only appears when the load is about 90% of the ultimate load (Fig. 16f) and debonding starts to propagate rapidly thereafter towards the free end of the FRP (Fig. 16g – 16i) leading to the total separation of the FRP plate from the concrete (Fig. 16j).

This debonding failure process is very similar for specimen No. 1 in Ali-Ahmad et al. (2006) (Fig. 17).

CONCLUSIONS

A concrete damage model based on the plastic degradation theory has been proposed and implemented into the concrete damage plasticity model in ABAQUS to simulate the FRP-to-concrete bond behavior in this paper. The plastic degradation is used to describe the damage of the concrete after it enters softening in both tension and compression. The damage effects are modeled in terms of plastic strain rather than the stiffness degradation. The proposed model has been implemented in ABAQUS to model the FRP-to-concrete bond behavior in the single shear test. A number of other damage models have also been investigated and their predictions as well as results from the proposed damage model have been compared with test data. The results have shown that the proposed model can accurately predict the bond behavior in the entire loading process and the numerical predictions are in closer agreement with test data from the literature than other models. The FE model also predicts that an increase of the bond length can lead to a small increase of the loading capacity even when the FRP bond length is larger than the effective bond length, as observed in some experiments.

ACKNOWLEDGMENTS

The first author acknowledges financial support received from the Research Grants of Xi'an University of Architecture and Technology (Project No: DB01153).

REFERENCES

ABAQUS (2007). ABAQUS Analysis user's manual, version 6.7.

ACI 318 (2002). "Building Code Requirements for Structural Concrete and Commentary ", ACI Committee 318.

Ali-Ahmad, M., Subramaniam, K. and Ghosn, M. (2006). "Experimental Investigation and Fracture Analysis of Debonding between Concrete and FRP Sheets." *Journal of Engineering Mechanics*, 132(9), 914-923.

Bažant, Z. and Jaime, P. (1998). *Fracture and Size Effect in Concrete and Other Quasibrittle Materials* CRC Press, Boca Raton, Florida.

Bažant, Z. and Oh, B. (1983). "Crack band theory for fracture of concrete." *Materials and Structures*, 16(3), 155-177.

Benvenuti, E., Vitarelli, O. and Tralli, A. (2012). "Delamination of FRP-reinforced concrete by means of an extended finite element formulation." *Composites Part B: Engineering*, 43(8), 3258-3269.

Benzarti, K., Freddi, F. and Frémond, M. (2011). "A damage model to predict the durability of bonded assemblies. Part I: Debonding behavior of FRP strengthened concrete structures." *Construction and Building Materials*, 25(2), 547-555.

Camata, G., Spacone, E., Al-Mahaidi, R. and Saouma, V. (2004). "Analysis of Test Specimens for Cohesive Near-Bond Failure of Fiber-Reinforced Polymer-Plated Concrete." *Journal of Composites for Construction*, 8(6), 528-538.

CEB-FIB (1991). "CEB-FIB MODEL CODE 1990." Thomas Telford.

Chen, G. M., Chen, J. F. and Teng, J. G. (2012). "On the finite element modelling of RC beams shear-strengthened with FRP." *Construction and Building Materials*, 32, 13-26.

Chen, G. M., Teng, J. G. and Chen, J. F. (2011). "Finite-Element Modeling of Intermediate Crack Debonding in FRP-Plated RC Beams." *Journal of Composites for Construction*, 15(3), 339-353.

Chen, J. F. and Pan, W. K. (2005). "Three dimensional stress distribution in FRP-to-concrete bond test specimens." *Construction and Building Materials*, 20(1-2), 46-58.

Chen, J. F. and Teng, J. G. (2001). "Anchorage Strength Models for FRP and Steel Plates Bonded to Concrete." *Journal of Structural Engineering*, 127(7), 784-791.

Chen, J. F., Yang, Z. J. and Holt, G. D. (2001). "FRP or steel plate-to-concrete bonded joints: effect of test methods on experimental bond strength." *Steel Compos Struct* 1(2), 231-244.

Chen, J. F., Yuan, H. and Teng, J. G. (2007). "Debonding failure along a softening FRP-to-concrete interface between two adjacent cracks in concrete members." *Engineering Structures*, 29(2), 259-270.

Cicekli, U., Voyiadjis, G. Z. and Abu Al-Rub, R. K. (2007). "A plasticity and anisotropic damage model for plain concrete." *International Journal of Plasticity*, 23(10-11), 1874-1900.

Coronado, C. A. and Lopez, M. M. (2007). "Damage Approach for the Prediction of Debonding Failure on Concrete Elements Strengthened with FRP." *Journal of Composites for Construction*, 11(4), 391-400.

Coronado, C. A. and Lopez, M. M. (2008). "Experimental Characterization of Concrete-Epoxy Interfaces." *Journal of Materials in Civil Engineering*, 20(4), 303-312.

Coronado, C. A. and Lopez, M. M. (2010). "Numerical Modeling of Concrete-FRP Debonding Using a Crack Band Approach." *Journal of Composites for Construction*, 14(1), 11-21.

Diab, H. and Wu, Z. (2007). "Nonlinear constitutive model for time-dependent behavior of FRP-concrete interface." *Composites Science and Technology*, 67(11-12), 2323-2333.

DIANA (2003). "DIANA User's Manual. 2nd ed. Delft, The Netherlands: TNO DIANA BV."

Godat, A., Neale, K. and Labossière, P. (2007). "Numerical Modeling of FRP Shear-Strengthened Reinforced Concrete Beams." *Journal of Composites for Construction*, 11(6), 640-649.

Grassl, P. and Jirásek, M. (2006). "Damage-plastic model for concrete failure." *International Journal of Solids and Structures*, 43(22-23), 7166-7196.

Hognestad, E. (1951). "A study of combined bending and axial load in reinforced concrete members (Bull. No. 399)." University of Illinois Engineering Experiment Station.

Hordijk, D. A. (1991). "Local Approach to Fatigue of Concrete." PhD Thesis, Delft University of Technology.

Lee, J. and Fenves, G. L. (1998). "Plastic-Damage Model for Cyclic Loading of Concrete Structures." *Journal of Engineering Mechanics*, 124(8), 892-900.

Lu, X. Z., Jiang, J. J., Teng, J. G. and Ye, L. P. (2006). "Finite element simulation of debonding in FRP-to-concrete bonded joints." *Construction and Building Materials*, 20(6), 412-424.

Lu, X. Z., Teng, J. G., Ye, L. P. and Jiang, J. J. (2005a). "Bond-slip models for FRP sheets/plates bonded to concrete." *Engineering Structures*, 27(6), 920-937.

Lu, X. Z., Ye, L. P., Teng, J. G. and Jiang, J. J. (2005b). "Meso-scale finite element model for FRP sheets/plates bonded to concrete." *Engineering Structures*, 27(4), 564-575.

Lubliner, J., Oliver, J., Oller, S. and Oñate, E. (1989). "A plastic-damage model for concrete." *International Journal of Solids and Structures*, 25(3), 299-326.

Marfia, S., Sacco, E. and Toti, J. (2012). "A coupled interface-body nonlocal damage model for FRP strengthening detachment." *Comput Mech*, 50(3), 335-351.

Mazars, J. and Pijaudier-Cabot, G. (1989). "Continuum Damage Theory-Application to Concrete." *J. Eng. Mech.*, 115(2), 345 – 365.

Menetrey, P. and Willam, K. J. (1995). "Triaxial Failure Criterion for Concrete and its Generalization." *ACI Structural Journal*, 92(3), 311-318.

MSC.Marc (2003). "User's manual." *MSC Software Corporation*.

Obaidat, Y. T., Heyden, S., and Dahlblom, O. (2010). "The effect of CFRP and CFRP/concrete interface models when modelling retrofitted RC beams with FEM." *Composite Structures*, 92(6), 1391-1398.

Pham, H. B. and Al-Mahaidi, R. (2007). "Modelling of CFRP-concrete shear-lap tests." *Construction and Building Materials*, 21(4), 727-735.

Pham, H. B., Al-Mahaidi, R. and Saouma, V. (2006). "Modelling of CFRP-concrete bond using smeared and discrete cracks." *Composite Structures*, 75(1-4), 145-150.

Rankine, W. J. (1857). "On the stability of loose earth." *Philosophical Transactions of the Royal Society of London*, 147, 9-27.

Rots, J. G. (1988). "Computational Modeling Of Concrete Fracture." Ph.D Thesis, Delft University of Technology, Delft.

Rots, J. G. (1991). "Smeared and discrete representations of localized fracture " *International Journal of Fracture* 51(1), 45-49.

Saenz, L. P. (1964). "Discussion of equation for the stress-strain curve of concrete-by Desayi, P. and Krishan, S." *ACI Journal* 61(9), 1229-1235.

Salomoni, V., Mazzucco, G., Pellegrino, C. and Majorana, C. (2011). "Three-dimensional modelling of bond behaviour between concrete and FRP reinforcement." *Engineering Computations*, 28(1), 5-29.

Smith, S., and Gravina, R. (2007). "Modeling Debonding Failure in FRP Flexurally Strengthened RC Members Using a Local Deformation Model." *Journal of Composites for Construction*, 11(2), 184-191.

Täljsten, B. (1996). "Strengthening of concrete prisms using the plate-bonding technique." *International Journal of Fracture*, 82(3), 253-266.

Teng, J. G., Chen, J. F., Simth, S. T. and Lam, T. (2002). *FRP-strengthened RC structures*, Wiley & Sons, UK.

Thorenfeldt, E., Tomaszewicz, A. and Jensen, J. J. (1987). "Mechanical properties of high strength concrete and application in design." In: *Proc., Symp. Utilization of High-Strength Concrete*, Stavanger, Norway.

Todeschini, C. E., Bianchini, A. C. and Kesler, C. E. (1964). "Behavior of Concrete Columns Reinforced with High Strength Steels." *ACI Journal Proceedings*, 61(6), 701-716.

Wu, Z. S., Yuan, H., Yoshizawa, H. and Kanakubo, T. (2001). "Experimental/Analytical Study on Interfacial Fracture Energy and Fracture Propagation Along FRP-Concrete Interface." *ACI International SP*, 201(8), 133-152.

Yang, Z. J., Chen, J. F. and Proverbs, D. (2003). "Finite element modelling of concrete cover separation failure in FRP plated RC beams." *Construction and Building Materials*, 17(1), 3-13.

Yang, Z.J. and Chen, J.F. (2005). “Finite element modelling of multiple cohesive discrete crack propagation in reinforced concrete beams.” *Engineering Fracture Mechanics*, 72(14), 2280-2297.

Yang, Z. J.; Su, X.T.; Chen, J.F. and Liu, G.H. (2009). “Monte Carlo simulation of complex cohesive fracture in random heterogeneous quasi-brittle materials.” *International Journal of Solids and Structures,* 46(17),3222-3234.

Yao, J., Teng, J. G. and Chen, J. F. (2005). "Experimental study on FRP-to-concrete bonded joints." *Composites Part B: Engineering*, 36(2), 99-113.

Yu, T., Teng, J. G., Wong, Y. L. and Dong, S. L. (2010). "Finite element modeling of confined concrete-II: Plastic-damage model." *Engineering Structures*, 32(3), 680-691.

Yuan, H., Teng, J. G., Seracino, R., Wu, Z. S. and Yao, J. (2004). "Full-range behavior of FRP-to-concrete bonded joints." *Engineering Structures*, 26(5), 553-565.

Table 1. Summary of FE studies on FRP-to-concrete bond behaviour

Reference	Concrete in compression	Concrete in tension	Concrete cracking	Remarks (Software)
Direct approach				
Lu et al. (2005b)	Hognestad's (1951) model	Linear softening	Smeared, fixed angle crack model	User defined shear retention model (MARC)
Lu et al. (2006)	User defined constitutive model		Smeared, rotating angle crack model	User defined constitutive model, 2-D plane stress assumption, (MARC)
	Saenz's (1964) model, Isotropic	exponential strain-softening, orthotropic		
Pham and Al-Mahaidi (2007)	Total strain crack model		Smeared, rotating angle crack model	(DIANA)
	Thorenfeldt et al.'s (1987) model	Hordijk's (1991) model		
Camata et al. (2004), Pham et al. (2006)	Nonlinear fracture mechanics-based model		Smeared & discrete crack model	Pre-defined cracking in concrete, Re-meshing technique (MERLIN)
	Menétrey and Willam's (1995) three-invariant plasticity model	Rankine's (1857) model		
Interface approach				
Diab and Wu (2007)	CEB-FIP (1991) model		Smeared crack model	Interface modeled (DIANA)
Salomoni et al. (2011)	Drucker-Prager constitutive law		Smeared crack model	Interface modeled based on Mazars' (1989) model (ABAQUS)
Crack band approach				
Coronado and Lopez (2007, 2010)	Todeschini et al.'s (1964) model for both plain concrete and crack band	Parameters of tension softening obtained from test for both plain concrete and crack band, bi-linear softening	Smeared crack model	Energy based damage model for tensile behavior in the crack band zone. No damage considered in other zones (ABAQUS)

Table 2. Loading capacity of typical specimens

Specimen Source	Concrete strength, MPa	Test, kN	FE prediction, kN	Chen and Teng's (2001) model, kN
II-5 Yao et al. (2005)	23	7.07	6.50	6.02
No. 1 Ali-Ahmad et al. (2006)	38	11.5	12.1	10.44
S-CFS-400-25 Wu et al. (2001)	57.6	14.1 (average of 3 specimens)	14.1	11.44

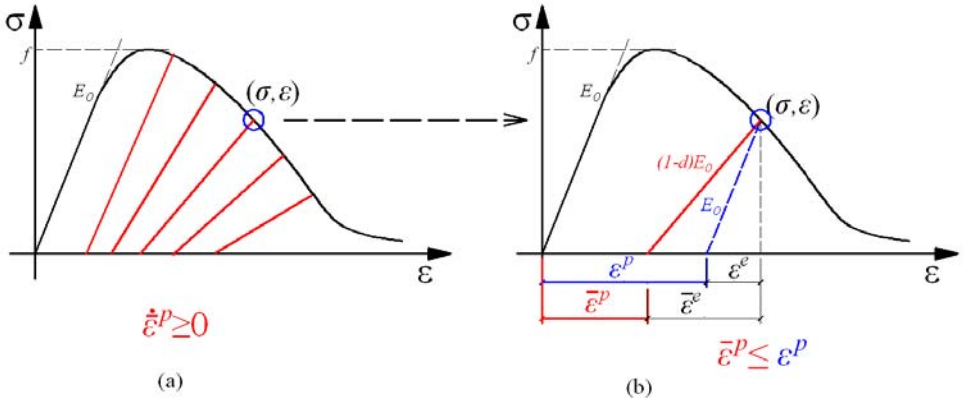

Figure 1. Damage plasticity model of concrete: (a) plastic strain degradation (b) damage definition

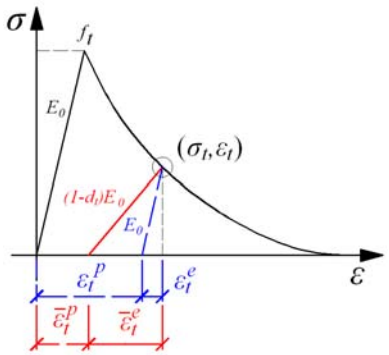

Figure 2. Stress-strain relationship of concrete under uniaxial tension

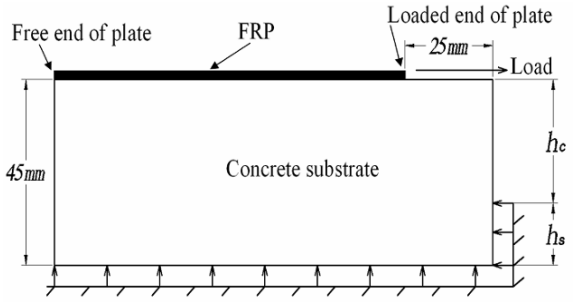

Figure 3. FE model of single shear test

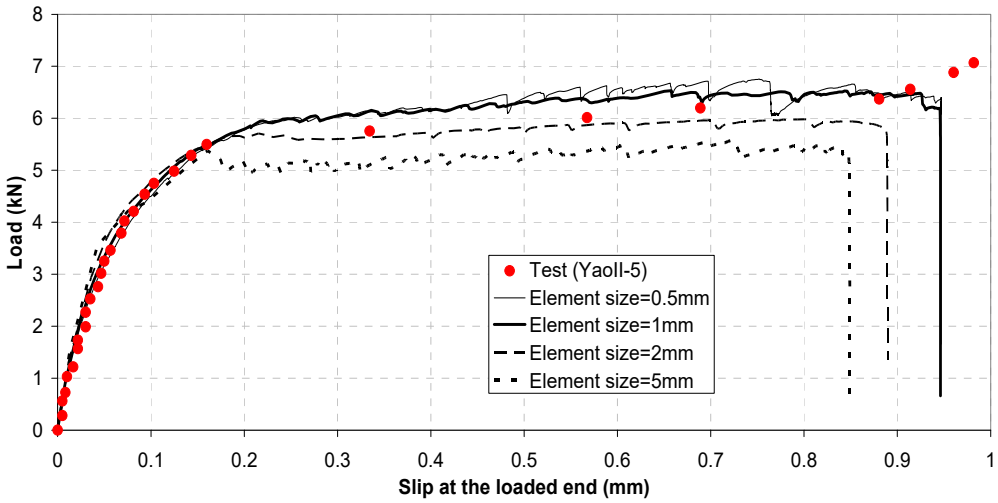

(a) Load-slip behavior

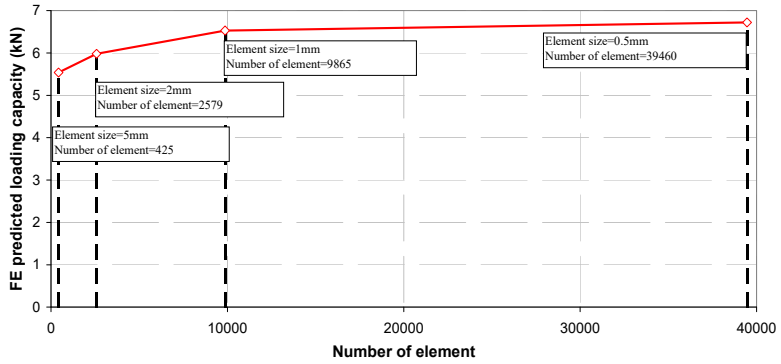

(b) Predicted loading capacity

Figure 4. Mesh convergence analysis for specimen II-5 in Yao et al. (2005)

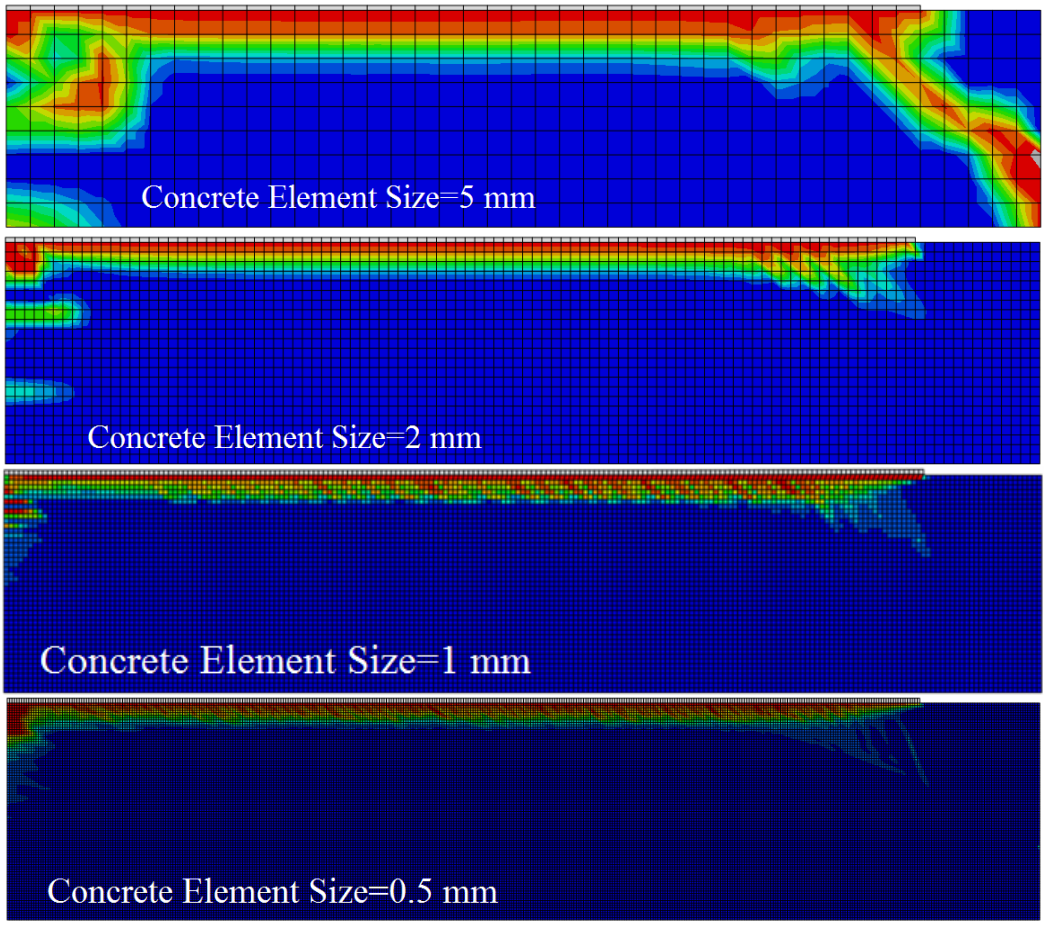

Figure 5. Effect of element size on predicted concrete damage contour: specimen II-5 in Yao et al. (2005)

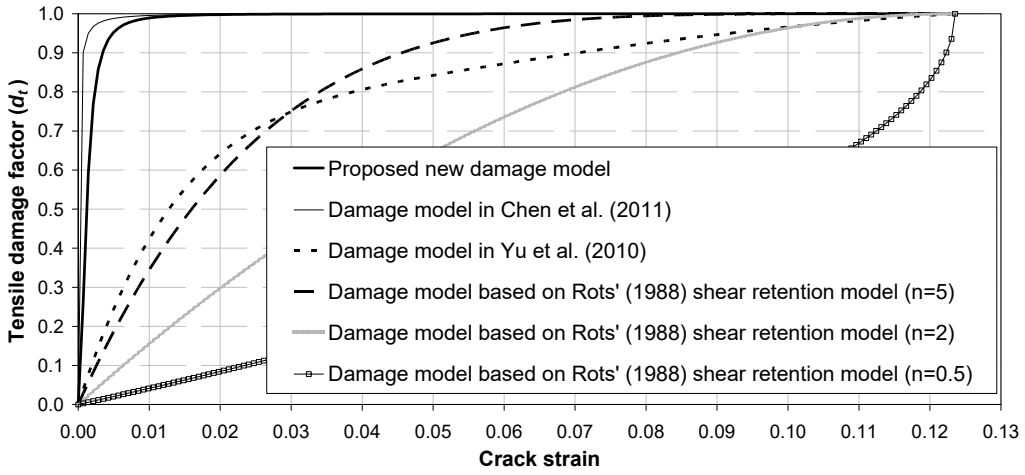

Figure 6. Tension damage models: for 1 mm element size and concrete strength as of specimen II-5 in Yao et al. (2005)

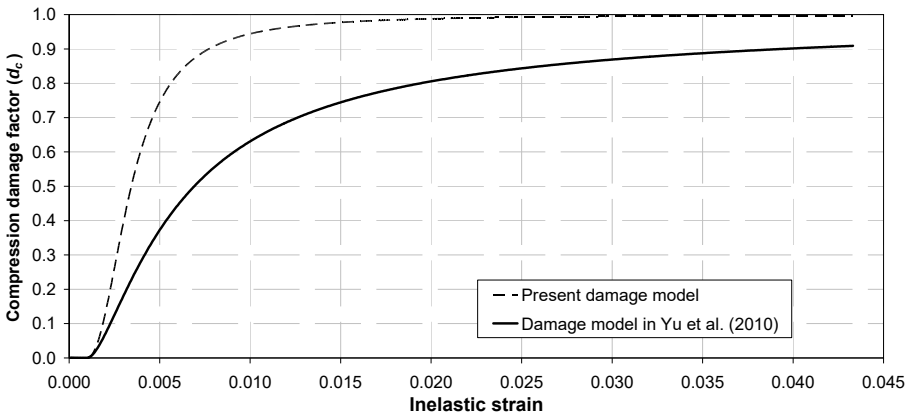

Figure 7. Compression damage models for 1 mm element size and concrete strength as of specimen II-5 in Yao et al. (2005)

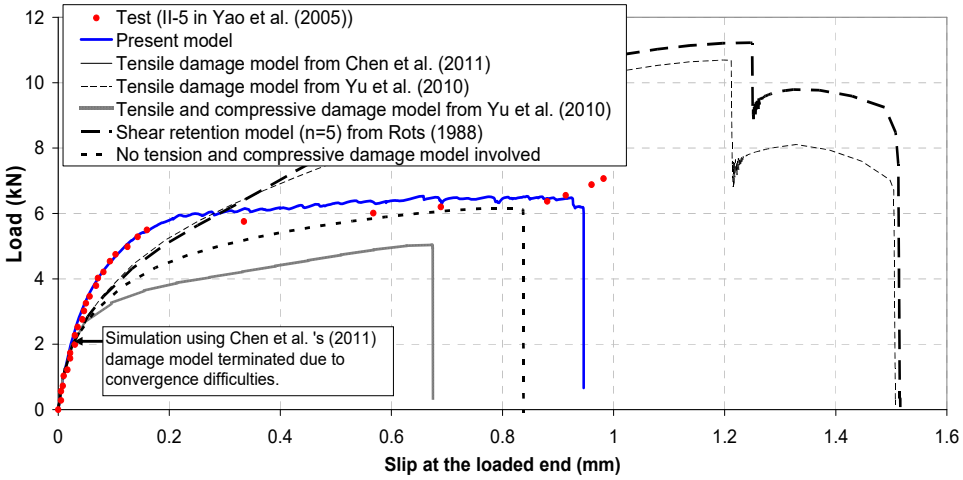

(a) Specimen II-5 in Yao et al. (2005)

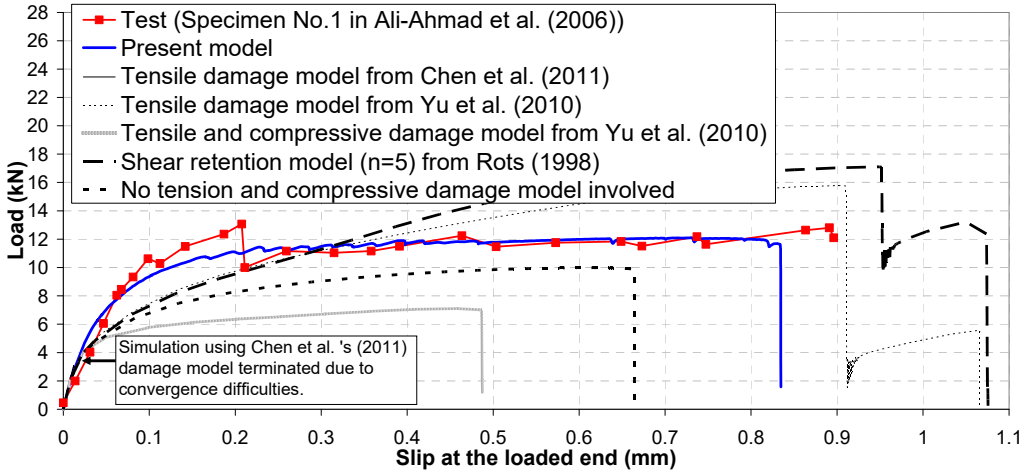

(b) Specimen No. 1 in Ali-Ahmad et al. (2006)

Figure 8. Effect of damage model on FE predicted load-slip curve

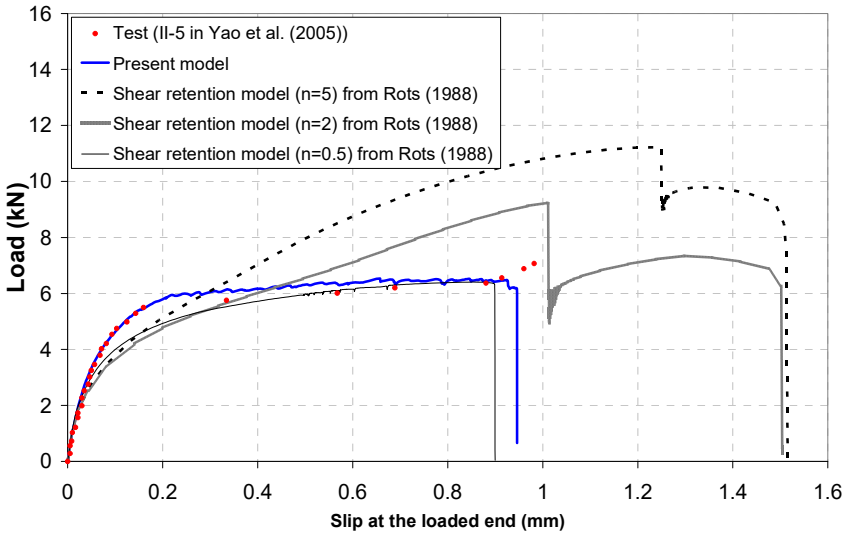

(a) Specimen II-5 in Yao et al. (2005)

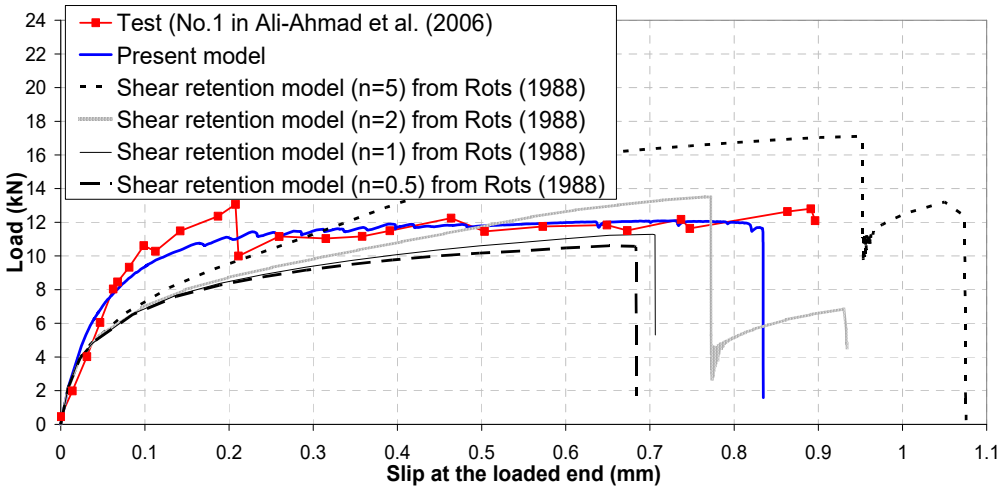

(b) Specimen No. 1 in Ali-Ahmad et al. (2006)

Figure 9. Effect of coefficient n in Rots' (1988) shear retention model on predicted load-slip curve

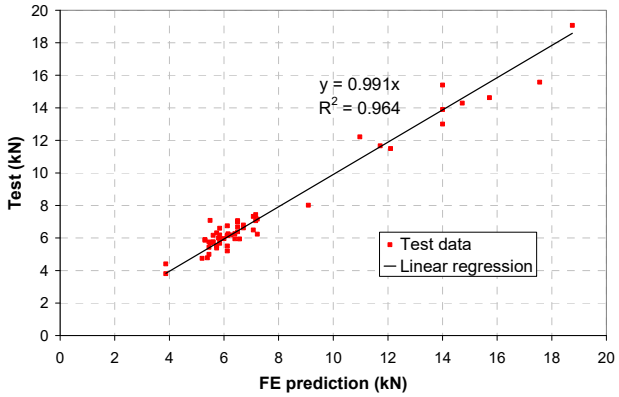

Figure 10. Comparison of FE prediction with test results

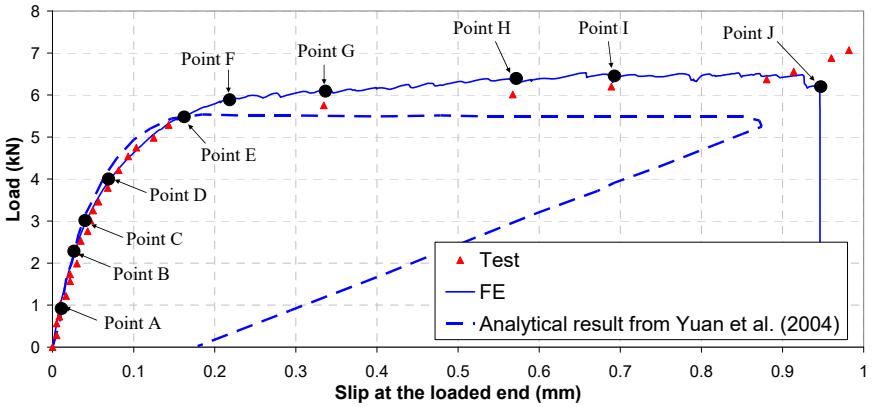

Figure 11. Comparison of FE prediction with test and analytical solution from Yuan et al. (2004): specimen II-5 in Yao et al. (2005)

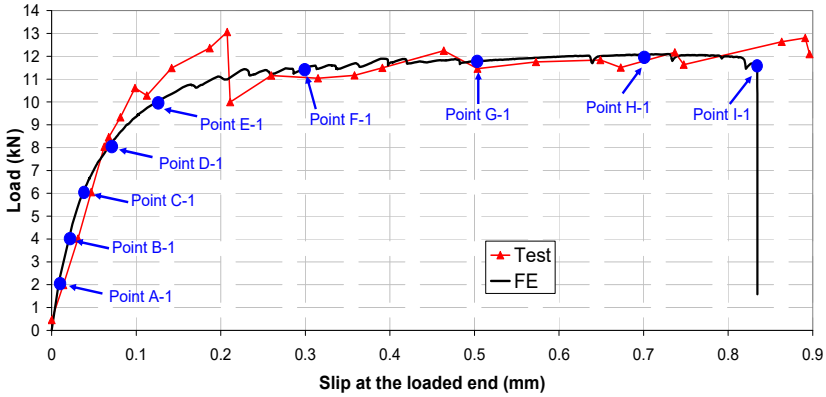

Figure 12. Comparison of FE prediction with test: specimen No. 1 in Ali-Ahmad et al. (2006)

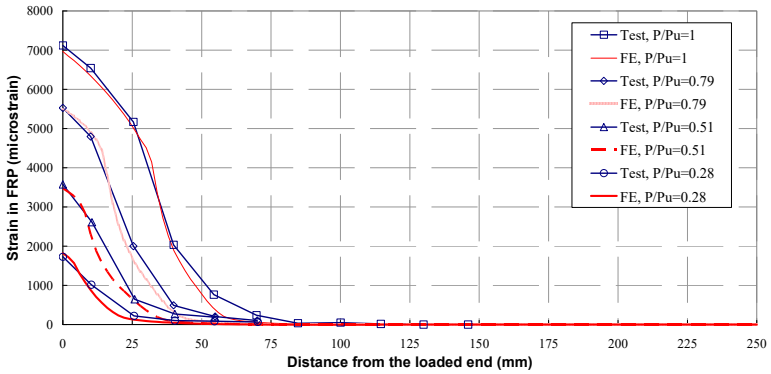

Figure 13. FE prediction and test FRP stain for specimen S-CFS-400-25 in Wu et al. (2001)

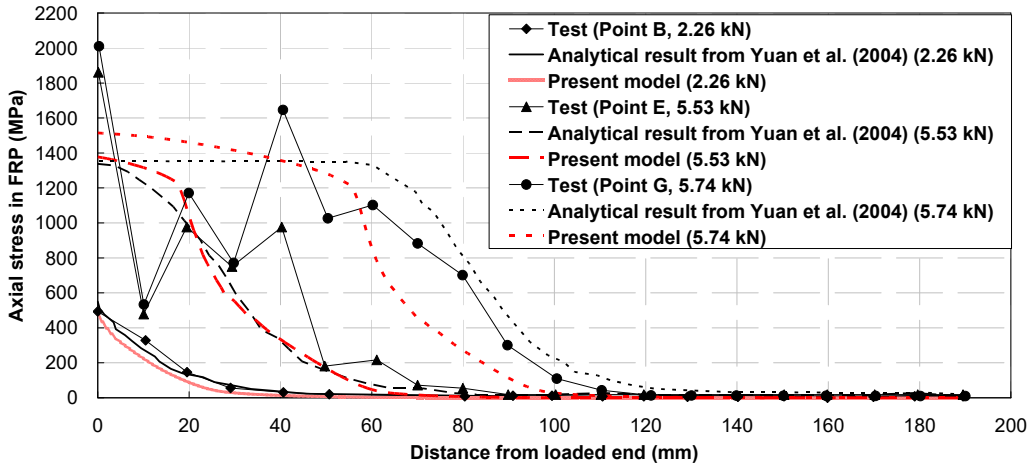

Figure 14. FE prediction, test and analytical solution of FRP axial stresses for specimen II-5 in Yao et al. (2005) corresponding to Points B, E and G on the load-slip curve in Fig. 11

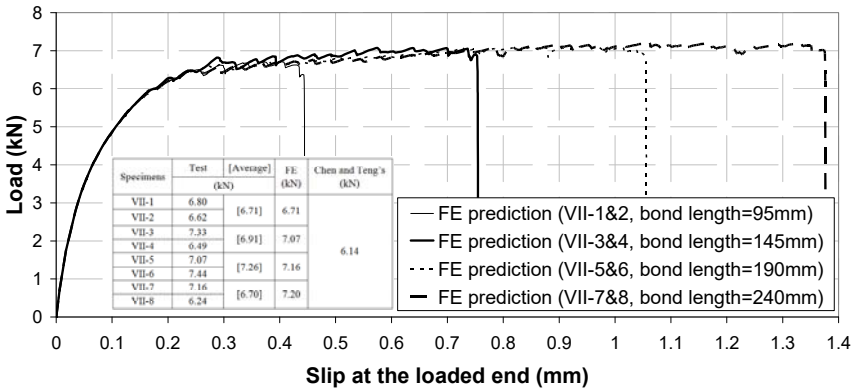

Figure 15. FE prediction on load-slip curves for specimens group VII in Yao et al. (2005)

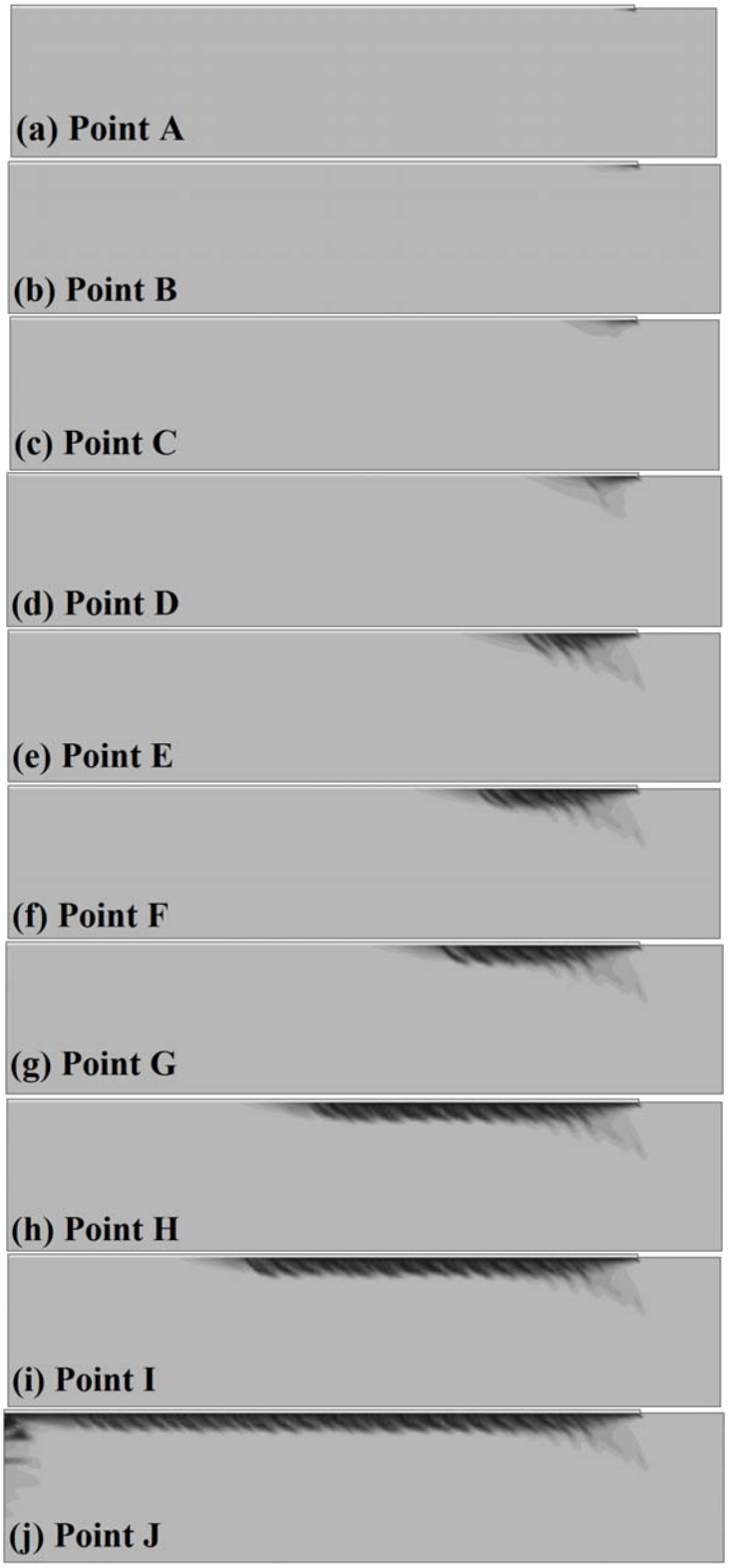

Figure 16. Propagation of debonding process: specimen II-5 in Yao et al. (2005) (Points A-J correspond to those in Fig. 11, scale the same as in Fig. 5)

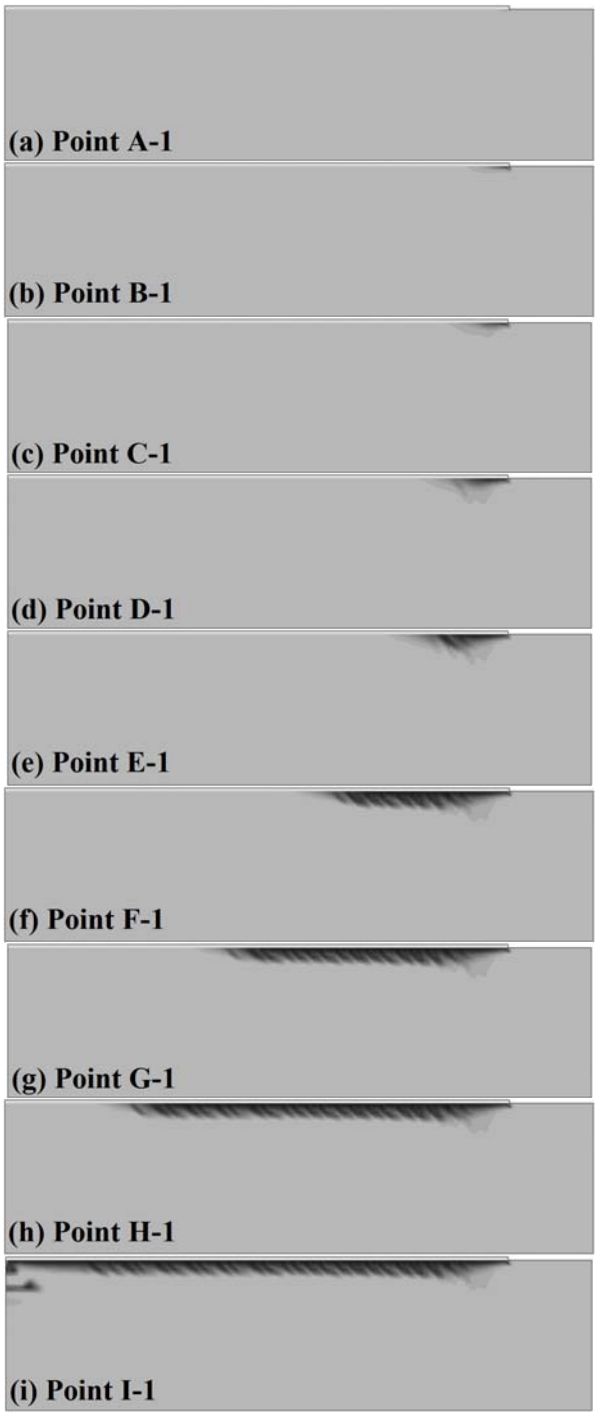

Figure 17. Propagation of debonding process: specimen No. 1 in Ali-Ahmad et al. (2006) (Points A-1 to I-1 correspond to those in Fig. 12, scale the same as in Fig. 5)